Applications of Wavelet Transform for Analysis of Freeway Traffic: Bottlenecks, Transient Traffic, and Traffic Oscillations

Zuduo Zheng[1], Soyoung Ahn[1*], Danjue Chen[2], and Jorge Laval[2]
[1]Arizona State University, [2]Georgia Institute of Technology

Abstract
This paper demonstrates the capabilities of wavelet transform (WT) for analyzing important features related to bottleneck activations and traffic oscillations in congested traffic in a systematic manner. In particular, the analysis of loop detector data from a freeway shows that the use of wavelet-based energy can effectively identify the location of an active bottleneck, the arrival time of the resulting queue at each upstream sensor location, and the start and end of a transition during the onset of a queue. Vehicle trajectories were also analyzed using WT and our analysis shows the wavelet-based energies of individual vehicles can effectively detect the origins of deceleration waves and shed light on possible triggers (e.g., lane changing). The spatiotemporal propagations of oscillations identified by tracing wavelet-based energy peaks from vehicle to vehicle enable analysis of oscillation amplitude, duration and intensity.
Keywords: Wavelet transform; Freeway bottleneck; Transition; Traffic oscillations

1 Introduction

Empirical studies of congested traffic often necessitate identifying key spatiotemporal features such as 1) bottleneck activations and spatiotemporal propagation of the resulting queues, 2) start and end times of phase transitions, and 3) origin and propagations of oscillation waves marking decelerations followed by accelerations. Researchers have developed several different techniques to investigate these features; these range from automated algorithms to process large amounts of data (Ban et al. 2007; Chen et al. 2004) to more manual methods to enhance the accuracy (Mauch and Cassidy 2002; Muñoz and Daganzo 2003). However, these techniques have noticeable limitations in terms of accuracy, efficiency, and/or reproducibility because of the noise in traffic data. Moreover, different techniques are employed depending on the features of interest, and thus a general tool to analyze all of the aforementioned features without compromising performance is desirable. Our study shows that WT (Daubechies 1992) is a powerful tool that is capable of analyzing the key features of congested traffic and addresses the shortcomings of existing methods.

WT is a time-frequency decomposition tool that is particularly effective in extracting local information from non-stationary time series. Unlike the Fourier transform (FT), WT provides both frequency (called scale in wavelet terminology) and time representation. Any local changes can be captured by moving the wavelet location and squeezing or dilating the wavelet window. Such a time-scale representation of the original time series data, which are often noisy and aperiodic, finds enormous applications in fluid mechanics, engineering testing and monitoring, medicine, finance, geophysics, network operations and other fields (Addison 2002; Crovella and Kolaczyk 2003).

WT has also been introduced to traffic engineering and intelligent transportation engineering. Combined with data mining techniques such as clustering, fuzzy logic, neural network, WT has

* Corresponding author. Civil, Environmental and Sustainable Engineering, Arizona State University, P.O. Box 875306, Tempe, AZ 85287-5306; Tel.: +1 480 965 1052; Fax: +1 480 965 0557;
Email address: sue.ahn@asu.edu.

been adopted to investigate various traffic-related issues, such as automatic detection of freeway incidents (Adeli and Samant 2000; Ghosh-Dastidar and Adeli 2003; Karim and Adeli 2002; 2003; Samant and Adeli 2000; 2001), traffic features around freeway work zones (Adeli and Ghosh-Dastidar 2004; Ghosh-Dastidar and Adeli 2006), traffic flow forecasting (Boto-Giralda et al. 2010; Jiang and Adeli 2005; Xie et al. 2007), and traffic pattern recognition (Jiang and Adeli 2004). These pioneering studies have demonstrated the potential of WT in analyzing non-stationary or noisy traffic data.

The primary objective of this paper is to demonstrate the potential applications of WT in identifying bottleneck activations, phase transitions, and oscillation evolutions through several examples of empirical analysis. Towards this end, this paper is organized as follows. Section 2 describes existing techniques to identify the aforementioned features of congested traffic and lists their advantages and shortcomings. Section 3 describes the theoretical background of WT and its adaptation to the analysis of traffic data. In Section 4, applications of WT for analyzing congested freeway traffic are demonstrated in detail through several case studies. Finally, Section 5 discusses conclusions and future research.

2 Background

2.1 Techniques to identify bottleneck locations and activation times

The simplest method to identify bottleneck locations and the spatiotemporal propagations of the resulting queues is by using raw traffic data (e.g., vehicle count, time-mean speed, or occupancy) from stationary traffic sensors. For instance, time-series speed curves reveal sensor locations that exhibit low speed values due to congestion. The approximate location of an active bottleneck is then identified as the section between the most downstream sensor location with congestion and its downstream neighbor (with no congestion). However, the bottleneck location and the arrival time of the queue at each upstream sensor location are often difficult to pinpoint with reasonable accuracy because of noise in traffic data. (The count data tend to be noisier than speed data.) Moreover, estimations of these features tend to be subjective, which raises the issue of reproducibility by other researchers. To partially smooth out noise and reveal underlying traffic patterns, raw traffic data can be aggregated over a certain time period before developing specific algorithms (Ban et al. 2007; Chen et al. 2004). However, the aggregation duration is selected arbitrarily, and the time resolution diminishes with aggregation.

Another widely used bottleneck analysis method is oblique cumulative curves (Cassidy and Bertini 1999). Cumulative curves of vehicle count, occupancy and speed are effective in suppressing noise, although changes in traffic patterns are not apparent due to their small scales relative to the characteristics analyzed. To overcome this shortcoming, cumulative curves are plotted with an oblique time axis (rather than a conventional orthogonal axis) to amplify temporal changes in traffic states. A bottleneck activation time (or a queue arrival time) is identified by locating a point where a sudden decrease in the slope of a cumulative vehicle speed or count curve occurs. This technique can smooth out the noise and reveal underlying traffic trends without compromising the original time resolution. However, it is difficult to entirely automate this procedure because one needs to adjust the degree of the oblique axis for different days, locations, and lanes to find the optimal degrees that best reveal traffic trends. Therefore, this method is time-consuming and labor-intensive, and thus unsuitable for analyzing many different days and locations. Moreover, the estimated event times are subjective because there is no objective standard to distinguish minor and major events, which raises a reproducibility issue.

Development of speed contours is another popular method that has been implemented in major archives such as the Performance Measurement System (PeMS 2008) and Portland Oregon Regional Transportation Archive Listing (PORTAL 2009). For a given stretch of roadway, traffic conditions are represented on a time-space plane by a color scheme corresponding to a range of speeds. Speed contours are an effective tool for preliminary analysis because they provide good spatial coverage and an overall picture of traffic evolution. However, it is difficult to determine precise event times in an objective manner.

2.2 Techniques to identify transitions

The start and end times of phase transitions during bottleneck activations are typically identified using raw traffic data, aggregated data, or oblique cumulative curves (Muñoz and Daganzo 2003; Sarvi et al. 2007), which suffer the limitations in the context as mentioned above. Using an empirical fundamental diagram (FD) (Muñoz and Daganzo 2003) is another way to analyze transitions. Raw or aggregated vehicle count (or flow) and occupancy pairs are plotted to obtain an empirical FD. Then the start of transition is identified as when flow-occupancy pairs start to drift from the uncongested to the congested branches of the empirical FD. The end of transition is identified as when the data points finally reach the congested branch. However, identifying precise event times can be rather subjective or inaccurate because of noise in the data and reduced data resolution.

2.3 Techniques to measure oscillations

Li et al. (2010) provide an excellent review of techniques to measure oscillations. One popular method in the time domain is to take the second-order difference of the cumulative data sequence (e.g. vehicle count, time-mean speed) with a moving time window (Mauch and Cassidy 2002; Ahn and Cassidy 2007). The motivation of this method is to remove noises in the data and de-trend longer-term changes in order to quantify local variations that are believed to be oscillations. Li et al. (2010) demonstrated (Fig.1 in their paper) that this method is sensitive to the choice of window length; with an inappropriate one, periodic oscillations may be dampened out, or Gaussian white noise may be distorted into a periodically oscillating sequence.

To overcome the shortcomings of the aforementioned technique in the time domain, Li et al. (2010) employed Short-Time Fourier Transform (STFT). STFT exploits the power of FT while remedying its poor performance for non-stationary signals. In this method, a signal is divided into time segments of the same length and then FT is applied to each time segment while assuming a stationary signal (Leon 1995). Using STFT, Li et al. identified stationary time intervals and then selected a dominant frequency to measure traffic oscillation's amplitude and duration in each interval. Although STFT showed a promising performance in Li et al. (2010), this process hinges partly on subjective judgment. For example, it is not always clear where stationary time intervals are located by looking at STFT-produced time-frequency plots. Additionally, more than one frequency is often found salient, and thus, selecting a single dominant frequency is not always justifiable.

Finally, the methods developed in the previous studies are intended to analyze oscillations using aggregated data from inductive loop detectors rather than trajectory data.

As we demonstrate hereon, the present study addresses the notable shortcomings of the existing methods to analyze important traffic features. More specifically, the merits of using WT-based method are: 1) it minimizes subjectivity in selecting event times, and thus the results are reproducible by others; 2) it enables efficient analyses of a large amount of data; 3) it

streamlines the analysis of congested traffic because it can be used for analyzing different features; and 4) it enables microscopic analysis of vehicle trajectories which tend to be very noisy due to driver differences. 4) is particularly notable given that propagations of oscillations are likely related to driver characteristics.

3 Methodology: Wavelet Transform

To overcome the inherent limitations of FT, such as sensitivity to noise and poor performance when applied to nonlinear problems, WT was developed in the 1980s (Daubechies 1992). A wavelet is a real or complex mathematical function, $\psi(t)$, that can transform continuous time series into various scale components. This study employs real wavelets, which must satisfy two basic conditions (Addison 2002):

Condition (1): $E = \int_{-\infty}^{\infty} |\psi(t)|^2 dt < \infty$, (1)

Condition (2): $\int_{-\infty}^{\infty} \psi(t) dt = 0$, (2)

where *E* is wavelet energy, which must be finite; Condition (2) implies that a wavelet must have a zero mean. A WT coefficient (output) of a continuous signal $x(t)$ is called a continuous wavelet transform (CWT), and its general formulation is

$$T(a,b) = w(a) \int_{-\infty}^{\infty} x(t)\, \psi(\frac{t-b}{a}) dt, \quad (3)$$

where a is a scale parameter that governs the dilation and contraction of the wavelet, and b is a translation parameter that governs the movement of the wavelet along the time dimension. This weighting function $w(a)$ is typically set to $1/\sqrt{a}$ to ensure that wavelets at all scales have the same energy. When $a = 1$ and $b = 0$, $\psi(t)$ is called the mother wavelet. Finding the optimal mother wavelet for a particular signal may have theoretical merit but is not critical in practice because several widely known wavelets (e.g., Haar, Daubechies, Mexican hat, Morlet, Coifman, etc.) are near-optimal and provide similar results for a wide variety of signals (Donoho 1993). In view of this, we select the Mexican hat wavelet, as defined in (4), for this research.

$$\psi(\frac{t-b}{a}) = [1 - \left(\frac{t-b}{a}\right)^2] e^{-\frac{(\frac{t-b}{a})^2}{2}} \quad (4)$$

Note from (4) that the Mexican hat mother wavelet ($a = 1$ and $b = 0$) is the second derivative of the Gaussian distribution function, $e^{-\frac{t^2}{2}}$. The Mexican hat wavelet is one of the most widely used, and its shape (see Figure 1 for $a = 1$ and $b = 0$) is typical of traffic oscillations.

Figure 1

As an aside, discrete wavelets are typically used in other studies because they are more efficient than continuous wavelets like the Mexican hat wavelet and enable inverse transform to restore the original data with noise filtered. In this study, we weigh accuracy more than efficiency in identifying event times (e.g., bottleneck activation times) and do not analyze the de-noised data through inverse transform. Thus, the Mexican hat wavelet was selected. Adeli (2005; 2008) describes discrete wavelet transform and its applications to the intelligent transportation systems.

For our applications, speed time series, $v(t)$, is a continuous signal function. A WT coefficient of $v(t)$ can be obtained by plugging (4) into (3):

$$T(a,b) = \frac{1}{\sqrt{a}} \int_{-\infty}^{\infty} v(t) \, [1 - \left(\frac{t-b}{a}\right)^2] e^{-\frac{(\frac{t-b}{a})^2}{2}} dt \quad (5)$$

Then, the average wavelet-based energy at b is computed based on the WT coefficients for different scales; i.e.,

$$E_b = \frac{1}{\max(a)} \int_0^{\infty} |T(a,b)|^2 da \qquad (6)$$

Note that E_b is computed based on $T(a, b)$ across different scales rather than the most dominant scale (as is the case in STFT). This capability is the unique strength of WT and enables an effective analysis of non-stationary signals such as time-series traffic data. The average wavelet-based energy, E_b, is dimensionless because $T(a,b)$ is dimensionless. From (6), an abrupt speed change over time generates a sharp increase in the temporal distribution of the wavelet-based energy. Thus, we can exploit the energy distribution to identify significant speed changes attributed to onsets and clearances of queues and to arrivals of oscillation waves.

Of note, b is typically selected based on the time resolution of the original signal, such that E_b is computed at all time steps. To compute E_b, a reasonable upper bound is assigned to a for computational efficiency. The maximum value of a should be small enough to capture the local details of the original signal[2].

Figure 2 illustrates a sample WT application using a vehicle trajectory. Figure 2(a) shows the speed plot of a vehicle (source: FHWA 2008), superimposed with an example Mexican hat wavelet in which a = 32 and b = 8.267. (Because the resolution of the original signal is 0.1 seconds, an a of 32 corresponds to 3.2 seconds in the time domain.) The speed at b = 8.267 is a local minimum (A in Figure 2(a)), that marks an abrupt speed change by the start of an acceleration. Figure 2(b) shows the WT coefficients, $T(a, b)$, computed for the original speed time series using Equation (5) for the entire range of b and a =32.

The WT coefficient at A' also marks a local minimum corresponding to the abrupt speed change at A. To obtain the temporal distribution of the energy, the absolute WT coefficients, $|T(a, b)|$, are obtained for different values of the scale parameter a. Figure 2(c) shows the contour of $|T(a, b)|$ with a ranging from 1 to 64; A'' denotes $|T(32, 8.267)|$. In this case, the maximum value of a is set at 64 (6.4 seconds in the time domain) to ensure that the wavelet window does not include more than one deceleration or acceleration phase. Lighter regions of the contour, such as the region surrounding A'', represent larger values of $|T(a, b)|$, which contribute to higher energy. Finally, the temporal wavelet-based energy distribution for the speed time series is computed using Equation (6), as shown in Figure 2(d). The figure clearly shows an energy peak at b=8.267 (A''' in the figure) as well as several other peaks that can be traced back to other abrupt speed changes in Figure 2(a). Note that rigorous mathematical proofs of WT's capability to detect abrupt changes in signals are beyond the scope of this paper. Meyer and Salinger (1995), Daubechies (1992), and Mallat (1999) provide mathematical details of the WT's principles.

Figure 2

[2] Selection of the maximum value of a is also governed by the "boundary effect," which is characterized by large WT coefficients at both ends of the signal range. This occurs because the signal range is finite, and the speed outside the signal range is assumed to be zero. Large WT coefficients are obtained at the boundaries where the signal shifts from zero to an actual speed value. As a increases, the boundary effect dominates the actual signal pattern for longer durations. Thus, the maximum value of a should be selected such that a significant proportion of the signal range is free of the boundary effect. An easy way to avoid the boundary effect is to extend the signal range by including more data and then discard the WT coefficients from the extended portions. This procedure is implemented in all the cases presented in this paper.

4 Applications

In this section, we demonstrate non-stationarity of the data used in this study to justify the use of WT and three applications of WT using real data: 1) identification of bottleneck locations and activation times, 2) identification of regime changes, and 3) identification and measurement of oscillations.

4.1 Stationarity of traffic data

Stationarity of a process is characterized by constant statistical parameters, such as mean and the standard deviation, over time (Challis and Kitney 1991). Traffic data are often non-stationary due to changes in demand and bottleneck capacity, merges and diverges, and other complex dynamics such as lane-changing and stop-and-go driving motions. Figure 3(a) shows a typical speed time-series (grey circles) from the loop detector data used in this study (these data are described in detail in Section 4.2). The dashed and the dotted lines respectively represent the cumulative mean and the cumulative standard deviation. It is clear that the mean and the standard deviation of speed change over time, indicating that the temporal process of speed is not stationary. Figure 3(b) shows a typical speed time series of a vehicle from the trajectory data used in this study (these data are described in Section 4.3). The cumulative mean and standard deviation also demonstrate non-stationarity of the temporal speed.

Figure 3

4.2 Application 1: Identification of bottleneck locations and activation times

A segment of US-101 (from milepost (MP) 10.248 to MP 24.552) in Los Angeles, California is used in this study (see Figure 4 for its schematic). Vehicle counts and occupancies were collected by loop detectors and aggregated every 30 seconds (PeMS 2008). Speed at each loop detector is estimated based on Equation (7) (Kockelman and Ma 2007) because it is not measured directly:

$$\hat{\bar{v}}_{l,t} = \left(\frac{C_{l,t}}{30/3600}\right) \times \left(\frac{\bar{l}_{l,t}+l_d}{5280\times OCC_{l,t}}\right), \qquad (7)$$

where
$\hat{\bar{v}}_{l,t}$: the estimated time-average speed at location l and time t,
$C_{l,t}$: the vehicle count,
$OCC_{l,t}$: the occupancy (%),
$\bar{l}_{l,t}$: the average vehicle length, and
l_d: the effective detection zone length.

The sum of $\bar{l}_{l,t}$ and l_d is also referred to as the effective vehicle length (Kockelman and Ma 2007), which is assumed to be 18 ft in our study. As Kwon et al. (2003) and Coifman (2001) show, the average effective vehicle length can change by time of day and tends to be bi-modal around effective lengths for passenger cars (around 20 ft) and larger vehicles (around 60 ft). However, because our method is designed to detect considerable temporal changes in speed, the accuracy of the estimated speed is not critical.

Figure 4

Figure 5(a) shows time-series speed plots for ten loop detector stations between MPs 17.127 and 26.592 of US 101 on September 1, 2009. Note that the speed plots at different locations are vertically separated by a factor proportional to the actual distances. The figure demonstrates the existence of an active bottleneck between MPs 18.567and 21.482 because the stations upstream of MP 18.567 exhibit substantial decreases in speed approximately from 15:00 to 20:00. However, the exact times of congestion onset and clearance[3] at each station are difficult to determine due to noise in the data.

Figure 5(b) is a speed contour of the same data in a time-space domain. The data were aggregated over 5 minutes to present a clearer pattern. In the figure, dark regions correspond to low speeds according to the scale given in the legend. The speed contour plot shows that the bottleneck activated a little after 15:30 at a location between MPs 18 and 20. It clearly shows the congested time-space region although it is hard to determine the times of congestion onset and clearance (especially in an automated manner). Nevertheless, speed contours are a useful tool for preliminary analysis (e.g., isolating a segment with congestion).

Figure 5(c) presents wavelet-based energy plots for the same speed data. Each curve shows the wavelet-based energy distribution at each station. The figure shows that the wavelet-based energy distributions are nearly uniform from MPs 17.127 to18.567, implying no state changes from 14:00 to 22:00. However, four noticeable energy spikes appear at the stations upstream of MP 18.567. Based on the energy distributions, we conclude that 1) the bottleneck is located between MPs 18.567 and 21.482; 2) upon bottleneck activation, the disturbance signaling the onset of the congestion arrived at each station at the time of the first energy spike (e.g. at 15:38 at MP 21.482). By tracing these times at different locations (see the arrow labeled “onset of congestion” in Figure 5(c)), one can identify the backward propagation of the shockwave. Similarly, the disturbance signaling queue clearance arrived at each location at the time of the third energy spike. It is interesting to note that the queue clearance is attributed to 1) an increase in bottleneck capacity as evidenced by a backward moving shock from MPs 21.482 to 23.402 and 2) a decrease in demand as evidenced by a forward moving wave from MPs 26.092 to 23.402.

We next demonstrate WT’s application in a more complicated scenario in which multiple bottlenecks exist on a freeway segment, and a more severe bottleneck overrides a less severe one upstream. Figure 6(a) and (b) respectively show time-series speed plots and a speed contour for nine stations between MPs 15.717 and 24.552 on October 27, 2009. Two bottlenecks can be identified from these figures with limited temporal and spatial resolutions.

Figure 6(c) shows wavelet-based energy distributions for the same speed data. The first energy spike, signaling the onset of congestion, occurred at MP 21.482 at 6:21 and propagated backward to other upstream stations. We also observe the propagation of another queue from a second bottleneck located downstream of MP 15.717. This second shock eventually propagated to the first bottleneck, that is, the queue from the downstream bottleneck spilled over to the upstream one.

Figure 5
Figure 6

[3] Note that the exact activation and deactivation times of this bottleneck are unknown since the exact bottleneck location cannot be obtained due to limitations in the spatial resolution of loop detector data.

4.3 Application 2: Measurement of regime transitions

A transitional regime is observed when traffic shifts from one state to another. We focus on the transition from a free-flow to a congested state when a bottleneck activates. In particular, WT is used to identify the start and end times of a transition, which are critical to studying bottleneck features such as capacity drops. We demonstrate that using WT can substantially simplify the task of identifying transition times.

For the example shown in Figure 5, the bottleneck is located between MPs 18.567 and 21.482, and the stations upstream of the bottleneck exhibit four energy spikes (see Figure 5(c)). The first energy spike (square in the figure) at each station represents the change from a free flow state to a transitional regime. The second energy spike (circle) marks the end of the transition, which represents the change from a transitional regime to a congested regime. Similarly, the third and the fourth energy spikes respectively represent the start and the end of another transitional regime from a congested to a free-flow state. Figure 7(a) shows the start and the end times of the transitions at each station and the average shockwave speeds computed based on these times (i.e., the slope of each trend line).

It is notable that the shock waves propagate backward nicely and that similar average shock speeds (~ 7.3 mph) are obtained using the start times and the end times. Figure 7(b) shows that the duration of the transitional regime at each station (transition end time – start time) is approximately 17.5 minutes, ranging from 15 to 18.5 minutes depending on the station.

Figure 7

The same method can be applied to the more complicated scenario shown in Figure 6. The shock propagation paths and the transition durations for this scenario are shown in Figure 8. Figure 8(a) reveals two distinctive shock propagation paths that originated at the two different bottlenecks. The average shock speeds at the first (upstream) and the second (downstream) bottlenecks are approximately 12.6 mph and 7.7 mph, respectively, and the transition durations are approximately 17 minutes and 21 minutes, respectively.

Figure 8

4.3 Application 3: Oscillations

Freeway traffic oscillations in congested traffic are characterized by recurring patterns of decelerations followed by accelerations. Many aspects of oscillations remain puzzling primarily because of limitations in data availability and analysis techniques. With recent developments in image processing techniques, several datasets of high-resolution vehicle trajectories (FHWA 2008) have become available to researchers, providing an unprecedented opportunity to study microscopic features of oscillations. Exploiting these data, we demonstrate that WT enables systematic investigations of certain microscopic features including their origins and propagations.

This study uses the vehicle trajectory data collected as part of FHWA's Next Generation Simulation (NGSIM) program (NGSIM 2008). The study site shown in Figure 9 is a 2100-ft section on US-101 southbound in Los Angeles, California (Note that the lane numbering is incremented from the left-most lane). Trajectory data were collected with the resolution of 10 records per second from 7:50 a.m. to 8:35 a.m. on June 15, 2005.

Figure 9

Oscillation Formation

We define an oscillation as a deceleration phase followed by an acceleration phase. Wavelet-based energy is used to identify the origins and triggers of deceleration waves. The basic idea is similar to that used in identification of bottlenecks and transitional regimes; that is, any dramatic speed change will produce an energy spike in the wavelet frame. By tracing back to the vehicle with the first noticeable energy spike, the origin of a deceleration wave can be identified.

Figure 10(a) shows vehicle trajectories on lane 1, US 101, which exhibit a formation of a deceleration wave. To identify the trigger of the deceleration wave, Figure 10(b) zooms in on trajectories around the origin. However, simply by looking at the trajectories, it is not apparent which vehicle initiated the deceleration wave. Figure 10(c), which shows the wavelet-based energy of each vehicle in Figure 10(b), reveals that the first energy peak occurred with vehicle 2389, a follower of two lane-changers, vehicles 2376 and 2384. Thus, we conclude that this deceleration wave was triggered by LCM.

Figure 10

Oscillation Propagation

Once the origin of an oscillation is identified, we study the propagation of the oscillation from vehicle to vehicle by tracing the paths of the deceleration and acceleration waves using WT. Again, the significant speed changes that occur upon the arrivals of the deceleration and acceleration waves accompany spikes in wavelet-based energy, enabling us to pinpoint the wave arrival times. Figure 11 shows the time-series speed (top) of a vehicle displaying oscillations (vehicle 1753 in the dataset) and the corresponding energy distribution (bottom). Based on the time-series speed, this vehicle underwent two complete oscillation cycles (a deceleration followed by an acceleration phase) as labeled in the figure. The time of each phase change corresponds to an energy peak in the energy distribution. A typical oscillation cycle consists of three energy peaks: 1) the arrival of a deceleration wave, 2) the arrival of an acceleration wave, and 3) the arrival of another deceleration wave. Thus, the propagation of an oscillation is identified by tracing these energy peaks for following vehicles.

Figure 11

Figure 12(a) shows the trajectories of a group of vehicles (including the one exemplified in Figure 11) that encountered several oscillations. The figure illustrates the propagation of one of the oscillations by tracing the energy peaks (circles in the figure) identified from the energy distributions of individual vehicles. The first propagation path denotes the passage of a deceleration wave, and the second and the third propagation paths indicate the passages of an acceleration wave and another deceleration wave, respectively. Thus, these three propagation paths complete an oscillation cycle. Note that the slope of each path represents the wave propagation speed and that the third path does not always exist because there may not be another deceleration wave. The average propagation speeds estimated via regression are 10.54 mph for the first, 10.28 mph for the second, and 8.74 mph for the third path. Figure 12(b) presents the durations of the decelerated state for the same group of vehicles, which are estimated as the durations between the first and the second energy peaks. The figure reveals that the duration of the decelerated state is relatively stable, with an average of approximately 13 seconds. Figure 12(c) presents the amplitude (measured as the speed difference between the first and the second

energy peaks). The figure reveals that the amplitude increases slightly for the first ten vehicles and then decreases. Finally, Figure 12(d) shows the intensity, which is estimated as the ratio of the amplitude to the duration. Note that the intensity measures the rate of speed decrease during a deceleration phase.

Figure 12

5 Conclusions and Future Research

WT is a time-frequency decomposition tool that is particularly effective in extracting local information from non-stationary time series. Using real traffic data, this paper demonstrates the capabilities of WT for analyzing important features related to bottleneck activations and traffic oscillations in a systematic and reproducible manner. In particular, the analysis of loop detector data from a freeway showed that the wavelet-based energy can effectively identify the location of an active bottleneck and the arrival time of the resulting queue at each upstream sensor location. The method was also shown to function effectively in a more complex scenario with multiple bottlenecks. Moreover, the wavelet-based energy clearly revealed the start and end of a transition during the onset of a queue.

Vehicle trajectories were also analyzed using WT. The wavelet-based energies of individual vehicles effectively showed the origins of deceleration waves and shed light on possible triggers (e.g., lane changing). The spatiotemporal propagations of the identified oscillations were then identified by tracing wavelet-based energy peaks from vehicle to vehicle. The identified propagation paths enabled analysis of oscillation amplitude, duration and intensity.

This tool will enable systematic investigations of reductions in bottleneck discharge flow, various characteristics of transient traffic, and the mechanism of oscillation growth in relation to driver behavior and lane-changing maneuvers. Discrete wavelets may be used for these in-depth analyses since they are useful for removing noise and reserving underlying trends in traffic data. Works in these regards are ongoing.

Acknowledgement

This research was funded by National Science Foundation. The authors acknowledge the anonymous reviewers for their valuable comments.

References

Adeli, H., Karim A., 2005. Wavelets in Intelligent Transportation Systems, Wiley.

Adeli, H., Jiang, X., 2008. Intelligent Infrastructure: Neural Networks, Wavelets, and Chaos Theory for Intelligent Transportation Systems and Smart Structures, CRC Press.

Adeli, H., Samant, A., 2000. An adaptive conjugate gradient neural network-wavelet model for traffic incident detection. Computer-Aided Civil and Infrastructure Engineering 15 (4), 251-260.

Adeli, H., Ghosh-Dastidar, S., 2004. Mesoscopic-wavelet freeway work zone flow and congestion feature extraction model. Journal of Transportation Engineering 130 (1), 94-103.

Addison, P. S., 2002. The Illustrated Wavelet Transform Handbook: Introductory Theory and Applications in Science, Engineering, Medicine and Finance, Taylor & Francis.

Ahn, S., Cassidy, M. J., 2007. Freeway traffic oscillations and vehicle lane-change maneuvers. In: Allsop, R.E., Bell, M.G.H., Heydecker, B.G. (Ed.), International Symposium of Transportation and Traffic Theory, Elsevier, Amsterdam, pp 691-710.

Ban, X. J., Chu, L., Benouar, H., 2007. Bottleneck identification and calibration for corridor management planning. Transportation Research Record: Journal of the Transportation Research Board 1999, 40-53.

Boto-Giralda, D., Díaz-Pernas, F., González-Ortega, D., Díez-Higuera, J., Antón-Rodríguez, M., Martínez-Zarzuela, M., Torre-Díez, I., 2010. Wavelet-based denoising for traffic volume time series forecasting with self-organizing neural networks. Computer-Aided Civil and Infrastructure Engineering 25 (7), 530-545.

Briggs, W. M., Levine, R. A., 1997. Wavelets and field forecast verification. Monthly Weather Review 125 (6), 1329-1341.

Cassidy, M. J., Bertini, R. L., 1999. Some traffic features at freeway bottlenecks. Transportation Research Part B 33 (1), 25-42.

Challis, R. E., Kitney, R. I., 1991. Biomedical signal processing (in four parts). Part 1 Time-domain methods. Medical & Biological Engineering & Computing 28, 509-524.

Chen, C., Skabardonis, A., Varaiya, P., 2004. Systematic identification of freeway bottlenecks. Transportation Research Record: Journal of the Transportation Research Board 1867, 46-52.

Coifman, B., 2001. Improved velocity estimation using single loop detectors. Transportation Research Part A 35 (10), 863-880.

Crovella, M. E., Kolaczyk, E. D., 2003. Graph Wavelets for Spatial Traffic Analysis. Proceedings of IEEE Infocom 2003, San Francisco, California

Daubechies, I., 1992. Ten Lectures on Wavelets, Society for Industrial and Applied Mathematics (SIAM).

Donoho, D. L., 1993. Unconditional bases are optimal bases for data compression and for statistical estimation. Applied and Computational Harmonic Analysis 1 (1), 100-115.

Farge, M., 1992. Wavelet transforms and their applications to turbulence. Annual Review of Fluid Mechanics 24, 395-458.

Ghosh-Dastidar, S., Adeli, H., 2003. Wavelet-clustering-neural network model for freeway incident detection. Computer-Aided Civil and Infrastructure Engineering 18 (5), 325-338.

Ghosh-Dastidar, S., Adeli, H., 2006. Neural network-wavelet microsimulation model for delay and queue length estimation at freeway work zones. Journal of Transportation Engineering 132 (4), 331-341.

Jiang, X., Adeli, H., 2004. Wavelet packet-autocorrelation function method for traffic flow pattern analysis. Computer-Aided Civil and Infrastructure Engineering 19 (5), 324-337.

Jiang, X., Adeli, H., 2005. Dynamic wavelet neural network model for traffic flow forecasting. Journal of Transportation Engineering 131 (10), 771-779.

Karim, A., Adeli, H., 2002. Incident detection algorithm using wavelet energy representation of traffic patterns. Journal of Transportation Engineering 128 (3), 232-242.

Karim, A., Adeli, H., 2003. Fast automatic incident detection on urban and rural freeways using wavelet energy algorithm, Journal of Transportation Engineering 129 (1), 57-68.

Katul, G., Vidakovic, B., 1996. The partitioning of attached and detached eddy motion in the atmospheric surface layer using Lorentz wavelet filtering. Boundary-Layer Meteorology 77 (2), 153-172.

Kockelman, K. M., Ma, J., 2007. Freeway speeds and speed variations preceding crashes, within and across lanes. Journal of the Transportation Research Forum 46 (1), 43-62.

Kwon, J., Varaiya, P., Skabardonis, A., 2003. Estimation of truck traffic volume from single loop detectors with lane-to-lane speed correlation. Transportation Research Record: Journal of the Transportation Research Board 1856, 106-117.

Leon, C., 1995. Time-Frequency Analysis: Theory and Applications. Prentice Hall.

Li, X., Peng, F., Ouyang Y., 2010. Measurement and estimation of traffic oscillation properties. Transportation Research Part B 44 (1), 1-14.

Mallat, S. G., 1999. A Wavelet Tour of Signal Processing, Academic Press.

Mauch, M., Cassidy, M. J., 2002. Freeway traffic oscillations: Observations and predictions. In: Taylor M. (Ed.), International Symposium of Transportation and Traffic Theory, Pergamon-Elsevier, Oxford, UK.

Meyer, Y., Salinger, D., 1995. Wavelets and Operators, Cambridge University Press.

Muñoz, J. C., Daganzo, C. F., 2003. Structure of the transition zone behind freeway queues. Transportation Science 37 (3), 312-329.

NGSIM, 2008. Next Generation Simulation. <http://www.ngsim.fhwa.dot.gov/> (05/08, 2008).

PeMS, 2008. Freeway performance measurement system. <https://pems.eecs.berkeley.edu/> (08/10, 2008).

PORTAL, 2009. Portland oregon regional transportation archive listing. <http://portal.its.pdx.edu/> (07/01, 2008).

Samant, A., Adeli, H., 2000, Feature extraction for traffic incident detection using wavelet transform and linear discriminant analysis, Computer-Aided Civil and Infrastructure Engineering 15 (4), 241-250.

Samant, A., Adeli, H., 2001, Enhancing neural network incident detection algorithms using wavelets, Computer-Aided Civil and Infrastructure Engineering 16 (4), 239-245.

Sarvi, M., Kuwahara, M., Ceder, A., 2007. Observing freeway ramp merging phenomena in congested traffic. Journal of Advanced Transportation 41 (2), 145-170.

Xie, Y., Zhang, Y., Ye, Z., 2007. Short-term traffic volume forecasting using Kalman filter with discrete wavelet decomposition. Computer-Aided Civil and Infrastructure Engineering 22 (5), 326-334.

4. Figure

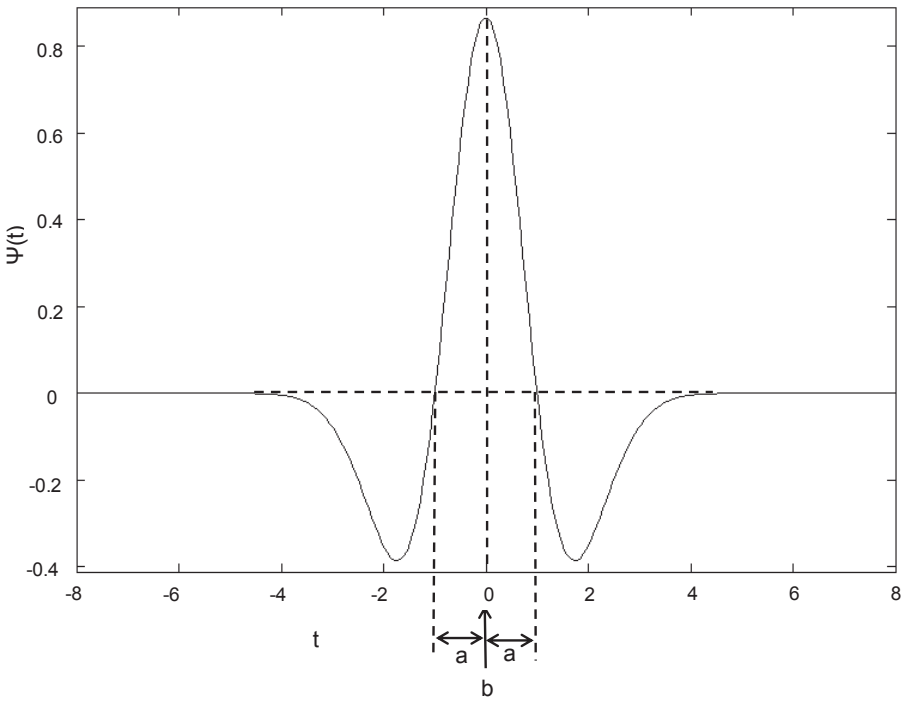

Figure 1 The Mexican hat mother wavelet.

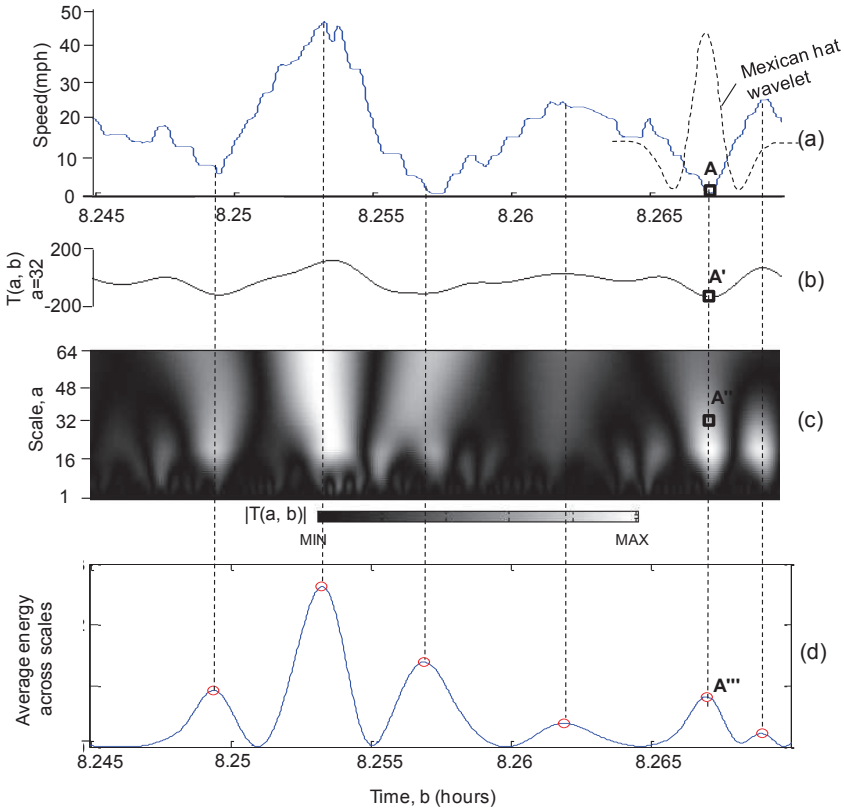

Figure 2 Illustration of wavelet transform and energy calculation
(a) Speed time series with a superimposed Mexican hat wavelet; (b) WT coefficients, $T(a, b)$, at scale a = 32; (c) Contour of the absolute values of WT coefficients, $|T(a, b)|$, from scale 1 to 64; (d) The temporal distribution of average wavelet-based energy across scales.

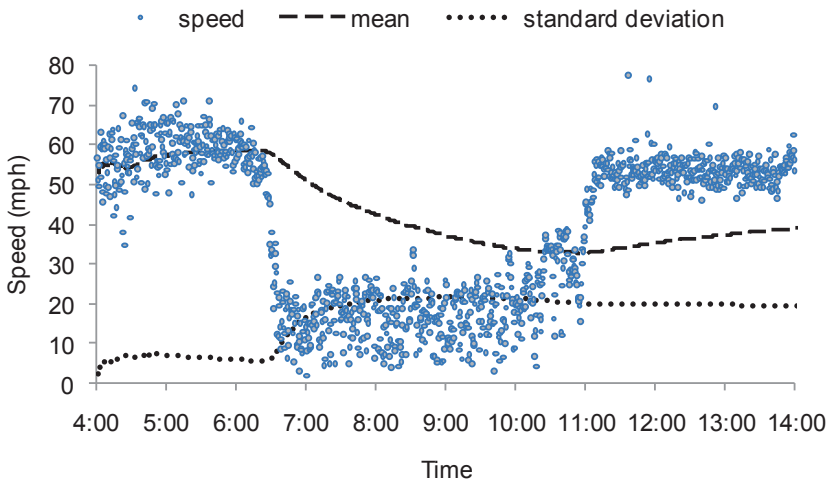

(a)

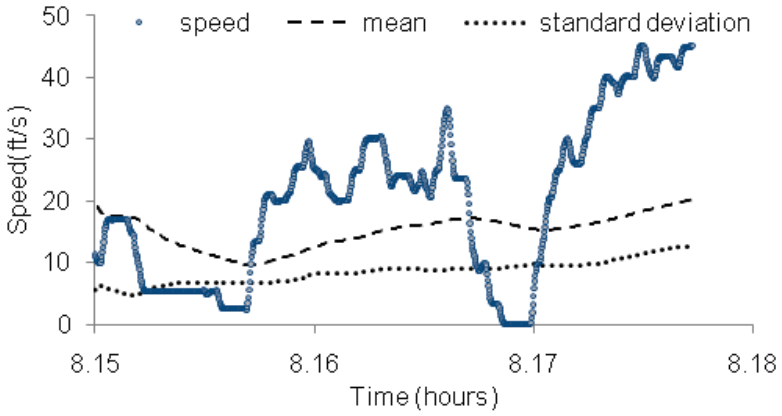

(b)

Figure 3 Illustration of non-stationarity of traffic data
(a) A typical speed time series from PEMS loop detector data (average over lanes, MP 21.482, US 101, October 27, 2009); (b) A typical speed time series of a vehicle from the NGSIM trajectory data (lane1, US 101).

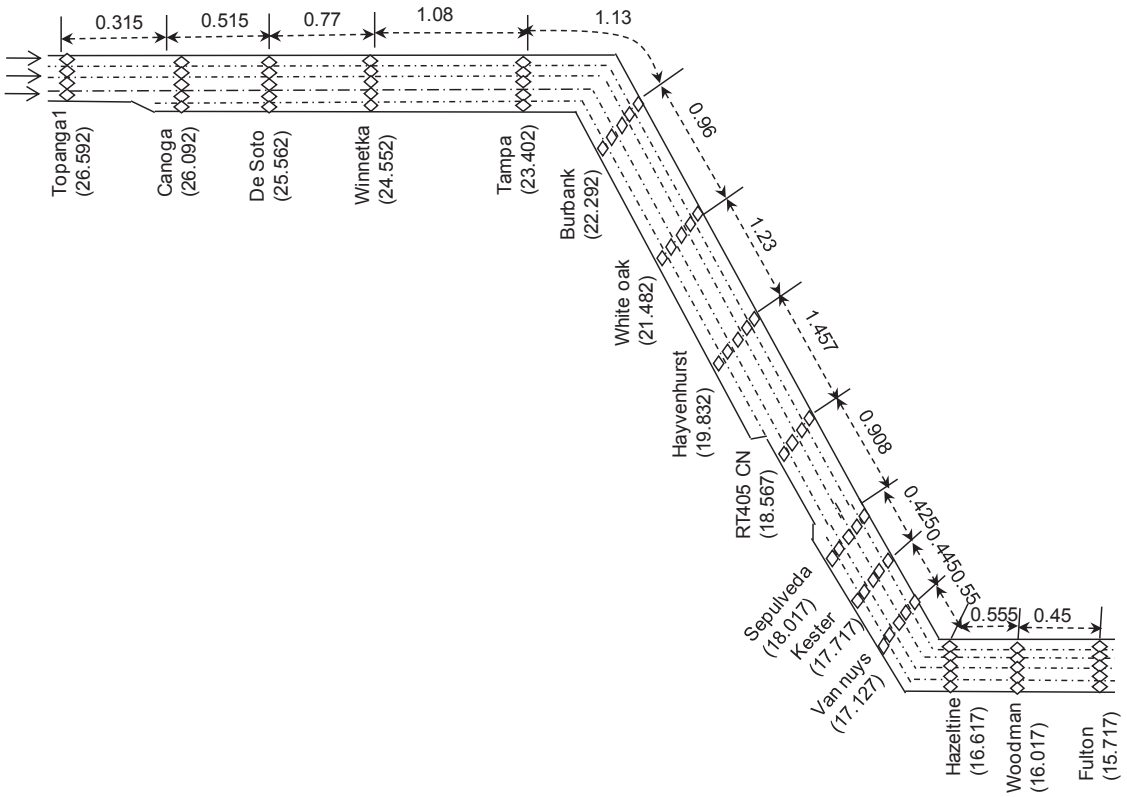

Figure 4 Schematic of US 101, MP 15.717 – MP 26.592 (Unit: miles).

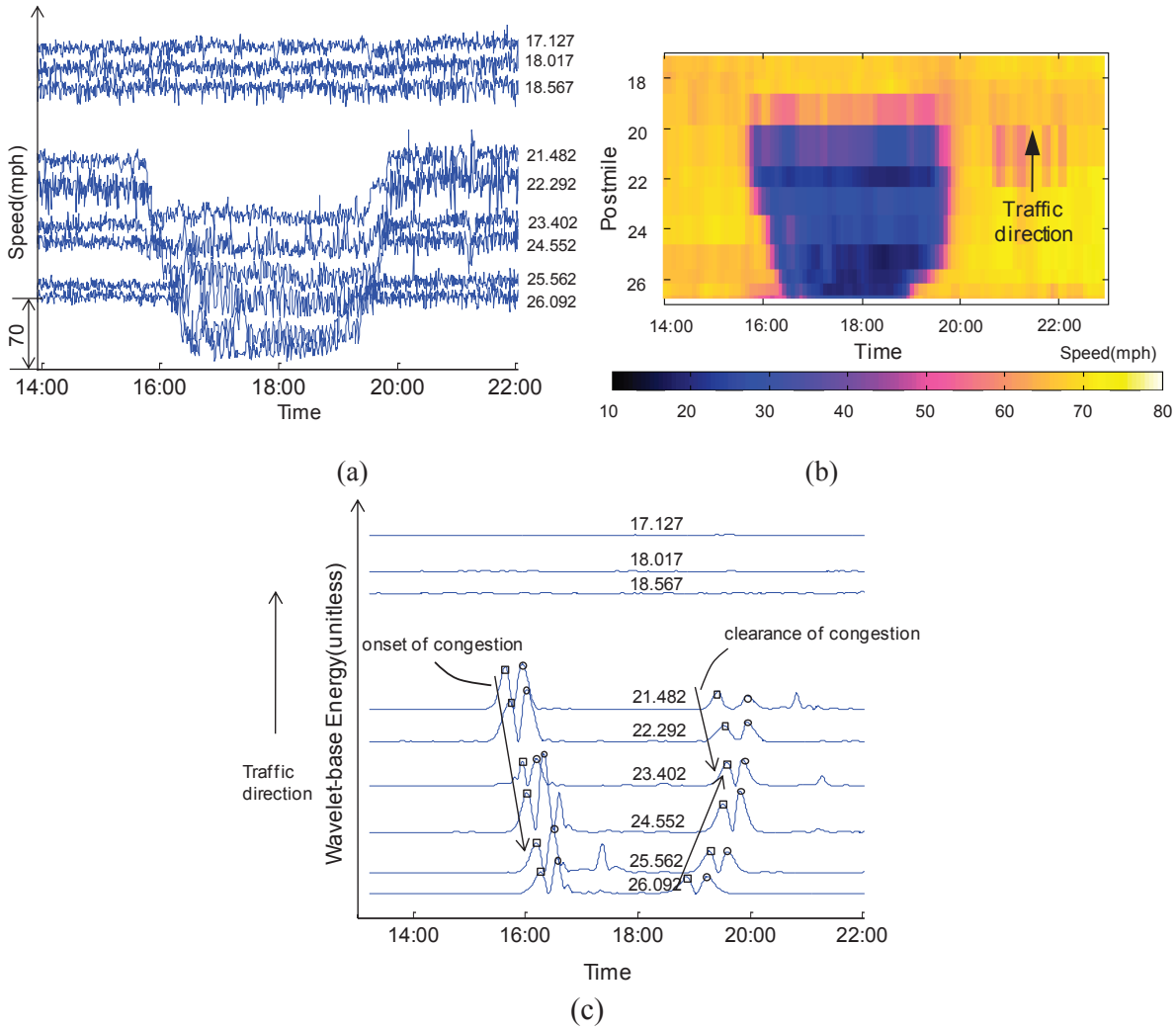

Figure 5 Identification of a bottleneck, US 101: September 1, 2009
(a) The raw speed plots; (b) The speed contour; (c) The wavelet-based energy distribution.

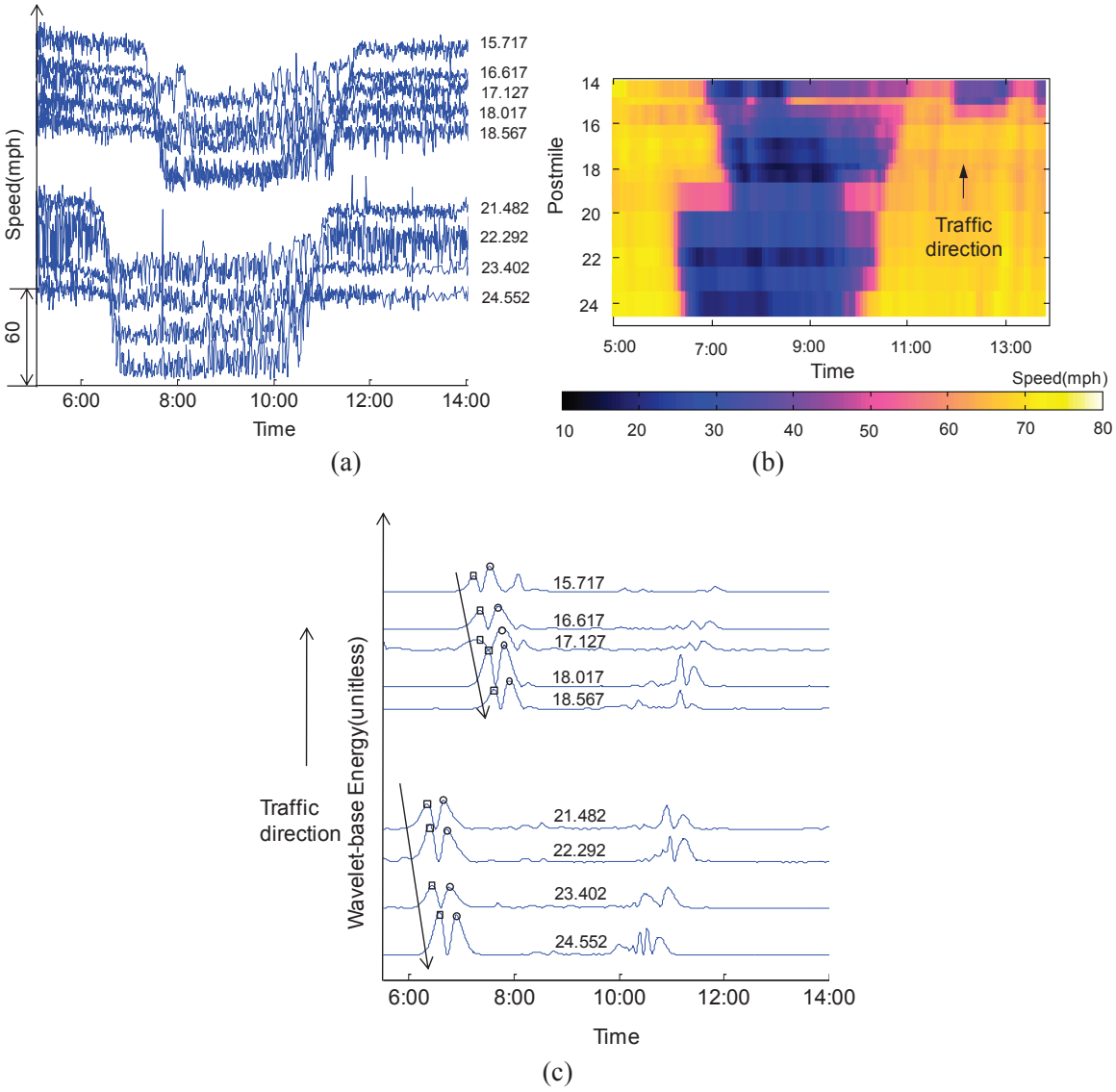

Figure 6 Identification of bottlenecks, US 101: October 27, 2009
(a) The raw speed plots; (b) The speed contour; (c) The wavelet-based energy distribution.

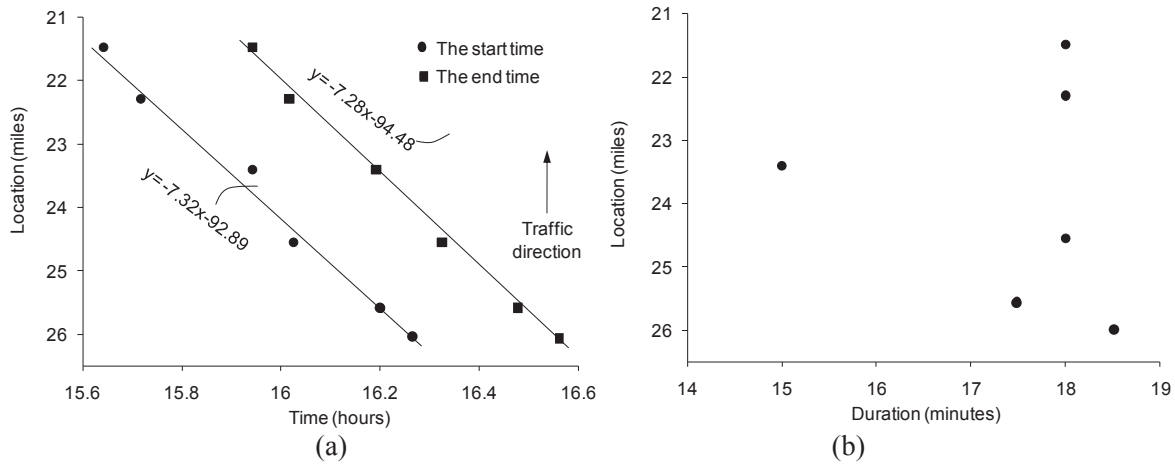

Figure 7 (a) The start and end times of the transition on September 1, 2009;
(b) The duration of the transition on September 1, 2009.

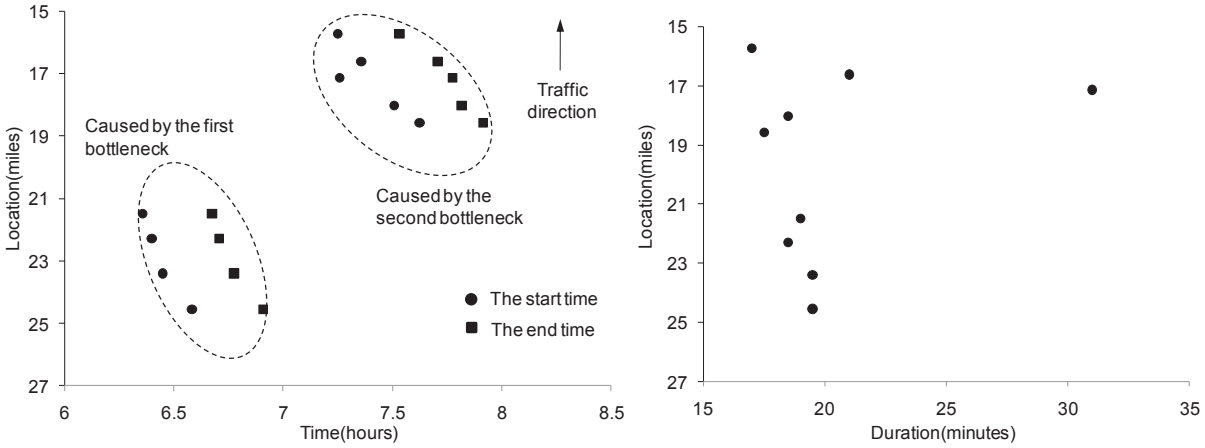

Figure 8 (a) The start and end times of the transition on October 27, 2009;
(b) The duration of the transition on October 27, 2009.

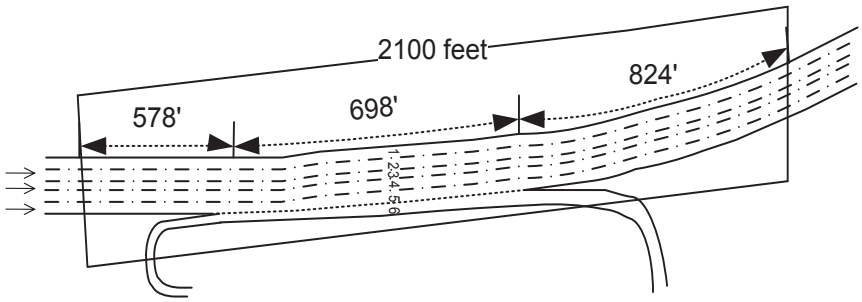

Figure 9 Schematic of a 2100 feet section of US 101.

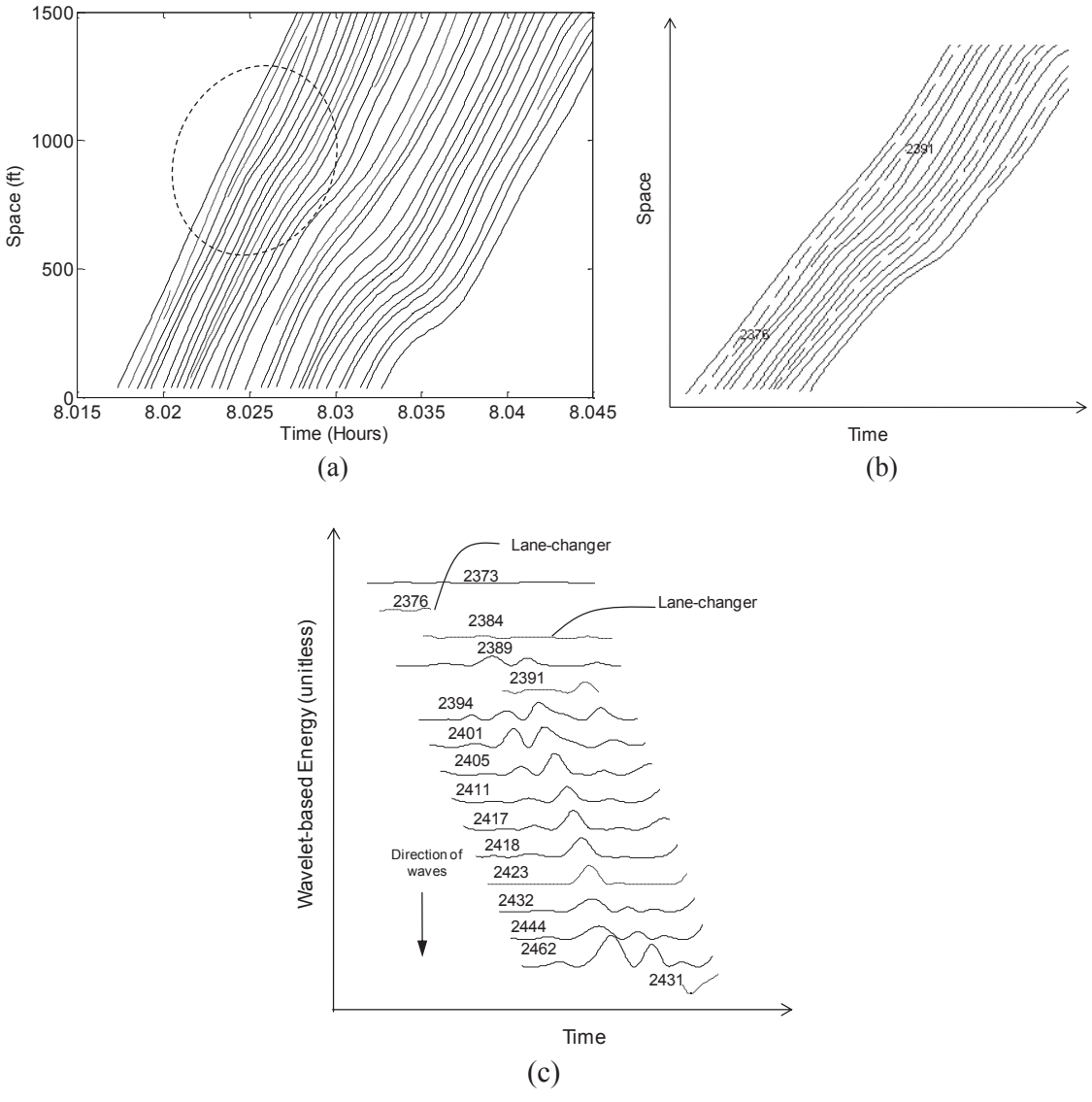

Figure 10 Example of an oscillation formation due to lane-changing maneuvers (lane 1, US 101) (a) Vehicle trajectories displaying a noticeable decelerated state; (b) Vehicle trajectories near the origin of the deceleration wave; (c) Temporal wavelet-based energy distributions of the vehicles near the origin of the deceleration wave.

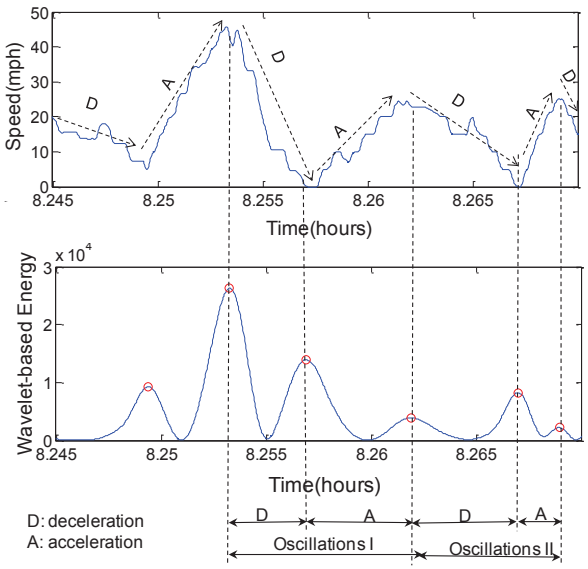

Figure 11 Illustration of oscillation measurement.

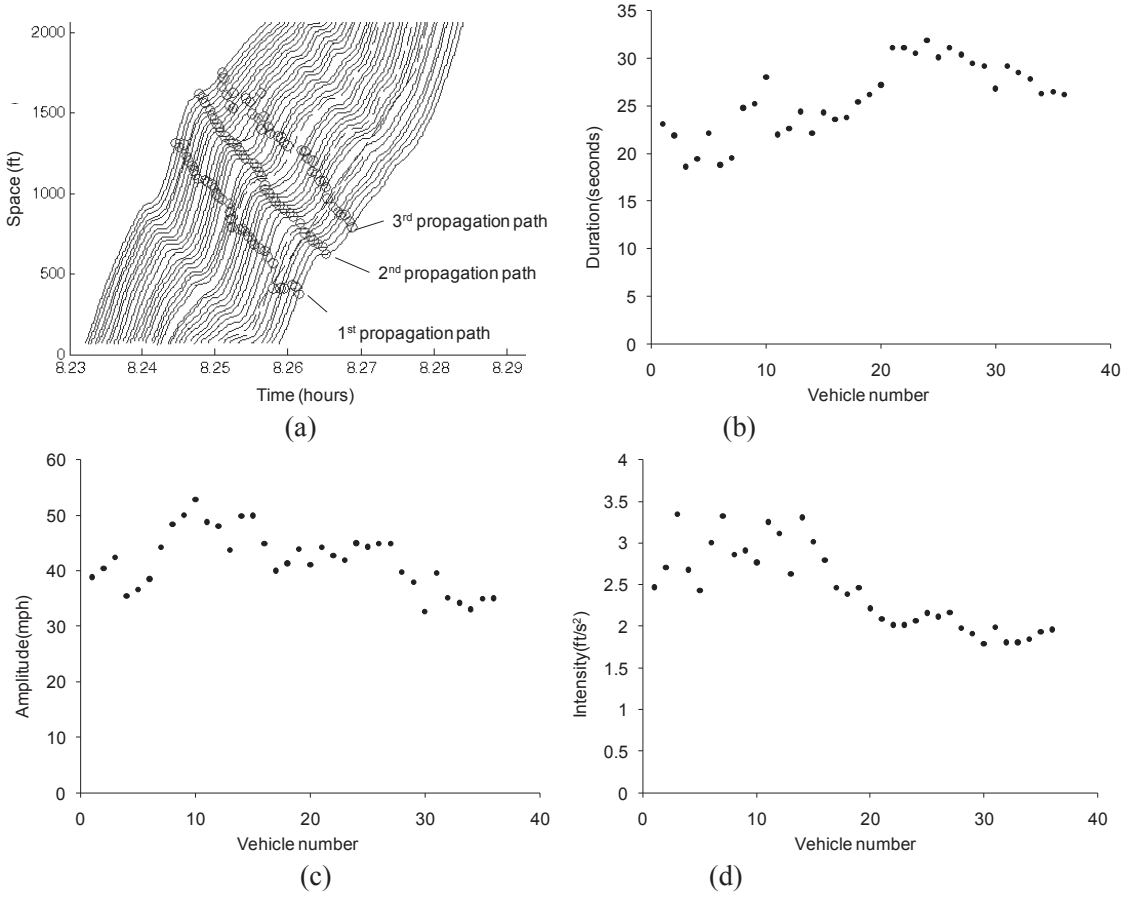

Figure 12 Example of an oscillation propagation on lane 1, US 101 (from 8:14 to 8:17 a.m.)
(a) Vehicle trajectories with three wave propagation paths identified using WT; (b) Oscillation durations measured based on the identified wave propagation paths; (c) Oscillation amplitudes; (d) Oscillation intensities.